Histochem Cell Biol (2012) 137:339–353
DOI 10.1007/s00418-011-0904-1

ORIGINAL PAPER

Epithelial sodium channels (ENaC) are uniformly distributed on motile cilia in the oviduct and the respiratory airways

Yehoshua Enuka · Israel Hanukoglu · Oded Edelheit · Hananya Vaknine · Aaron Hanukoglu

Accepted: 14 December 2011 / Published online: 30 December 2011

Abstract Epithelial sodium channels (ENaCs) are located on the apical surface of cells and funnel Na^+ ions from the lumen into the cell. ENaC function also regulates extracellular fluid volume as water flows across membranes accompanying Na^+ ions to maintain osmolarity. To examine the sites of expression and intracellular localization of ENaC, we generated polyclonal antibodies against the extracellular domain of human α-ENaC subunit that we expressed in E. coli. Three-dimensional (3D) confocal microscopy of immunofluorescence using these antibodies for the first time revealed that ENaCs are uniformly distributed on the ciliary surface in all epithelial cells with motile cilia lining the bronchus in human lung and female reproductive tract, all along the fimbrial end of the fallopian tube, the ampulla and rare cells in the uterine glands. Quantitative analysis indicated that cilia increase cell surface area >70-fold and the amount of ENaC on cilia is >1,000-fold higher than on non-ciliated cell surface. These findings indicate that ENaC functions as a regulator of the osmolarity of the periciliary fluid bathing the cilia. In contrast to ENaC, cystic fibrosis transmembrane conductance regulator (CFTR) that channels chloride ions from the cytoplasm to the lumen is located mainly on the apical side, but not on cilia. The cilial localization of ENaC requires reevaluation of the mechanisms of action of CFTR and other modulators of ENaC function. ENaC on motile cilia should be essential for diverse functions of motile cilia, such as germ cell transport, fertilization, implantation, clearance of respiratory airways and cell migration.

Keywords Extracellular fluid · Immunohistochemistry · Ion channels · Lung · Pseudohypoaldosteronism · Tubulin · Axoneme · CFTR

Y. Enuka · I. Hanukoglu (✉) · O. Edelheit
Department of Molecular Biology, Ariel University Center, Ariel 40700, Israel
e-mail: mbiochem@gmail.com

H. Vaknine
Division of Pathology, E. Wolfson Medical Center, Holon, Israel

A. Hanukoglu
Department of Pediatrics, Sackler Medical School, Tel-Aviv University, Tel Aviv, Israel

A. Hanukoglu
Division of Pediatric Endocrinology, E. Wolfson Medical Center, Holon, Israel

Introduction

A cilium is a thin finger-like extension on the cellular surface. It is covered by a bilayer membrane and has a microtubular skeleton that is called an axoneme. Microvilli extensions seen in many cell types, such as enterocytes, are fundamentally different from cilia and do not have a microtubule skeleton (Lange 2011). In mammalian cells, there are two types of cilia, motile and primary (Satir and Christensen 2007; Rohatgi and Snell 2010; Ishikawa and Marshall 2011). Motile cilia appear as tufts on the surface of epithelial cells that line body cavities in three organs: oviduct that transfers the ova from the ovary to the uterus, respiratory airways in the lung and brain ventricles (Lyons et al. 2006; Shah et al. 2009). Rhythmic beating of these cilia propels the fluid around the cilia. A variety of developmental and degenerative diseases collectively called "ciliopathies" have been associated with malfunction of the components of cilia (Hildebrandt et al. 2011).

The volume and the composition of the fluid bathing the cilia are crucial for motile cilia function (Widdicombe

2002; Marshall and Kintner 2008). A major determinant of fluid flow in biological fluids is the relative osmolarity of the extracellular and intracellular liquids (Bourque 2008). In vertebrates, sodium ion and its counter-ions are the major determinants of the osmolarity of the interstitial fluid (ISF) and blood (Takei 2000). Therefore, changes in Na^+ concentration affect both the volume and the flow of water across membranes to maintain osmolarity, and the volume of interstitial fluid. Studies in airway epithelial cultures from normal subjects and cystic fibrosis patients indicate that both Cl^- secretion and Na^+ absorption are required for maintenance of normal airway surface liquid volume (Tarran et al. 2006; Song et al. 2009).

On the apical (luminal) side of epithelial cells lining the kidney tubules, colon, respiratory airways and exocrine glands, the major gateway for the entry of Na^+ into cells is ENaC-type sodium channels (Kleyman et al. 2009; Rossier and Stutts 2009). These channels are composed of three homologous subunits encoded by three different genes (Chang et al. 1996; Saxena et al. 1998; Kashlan and Kleyman 2011). We previously demonstrated that mutations that lead to loss of function of ENaC result in hyponatremia and consequently severe dehydration in multi-system pseudohypoaldosteronism (PHA) (Chang et al. 1996; Strautnieks et al. 1996; Edelheit et al. 2005, 2010). Low expression of ENaC in the respiratory tract also disrupts clearance of lung fluid and may lead to respiratory distress in pre-term infants (Helve et al. 2007). Alpha-ENaC-deficient mice die because of defective lung liquid clearance (Hummler et al. 1996). In some of its pulmonary manifestations PHA resembles cystic fibrosis that results from mutations in the cystic fibrosis transmembrane conductance regulator (CFTR) gene (Hanukoglu et al. 1994; Kerem et al. 1999) that functions as a Cl^- channel (Li and Naren 2010; Riordan 2008). In the absence of a functional CFTR, ENaC leads to hyper-absorption of Na^+ and consequently dehydration of the mucus in the airways of cystic fibrosis patients (Riordan 2008). Transgenic mice that over-express β-ENaC display symptoms similar to cystic fibrosis including airway surface liquid (ASL) depletion, reduced mucus transport and chronic airway inflammation (Zhou et al. 2011).

Despite the expected importance of ENaC in the regulation of motile cilia function, there is currently no information on the association of ENaC with cilia. Most of the reports on the localization of ENaC in various epithelial cells are based on mRNA quantitation (Duc et al. 1994; Boyd and Naray-Fejes-Toth 2007). Immunohistochemical images of ENaC expression are mostly of low resolution or unclear (Duc et al. 1994; Biner et al. 2002). In most tissues where ENaC is expressed, we have little knowledge of the specific distribution of ENaC in different cell types that populate each epithelia. There is evidence that ENaC is expressed in the airway epithelia and uterus (Gaillard et al. 2000; Yang et al. 2004), but, there is no knowledge of the subcellular localization of ENaC in tissues with motile cilia. The reason for this is that until now, the antibodies used for the localization of ENaC have been generated against short synthetic peptides such as α-ENaC intracellular N-terminus (Masilamani et al. 1999) that is cleaved by an ENaC activating furin serine protease (Kleyman et al. 2009; Hu et al. 2009).

In this study, we expressed and isolated extracellular domains of ENaC subunits and generated polyclonal antibodies against these domains. These antibodies for the first time permit direct high resolution visualization of intracellular sites of localization of ENaC. Immunohistochemical analyses using the antibodies reveal that epithelial sodium channels are uniformly distributed on all motile cilia surfaces. To the best of our knowledge, this is the first study to document abundant and uniform distribution of an ion channel on all motile cilia in different cell types. These findings have important implications for the mechanism of regulation of pericilial fluid by ion channels.

Materials and methods

Cloning, expression and isolation of ENaC subunit extracellular domains in *E. coli*

All cDNAs used in this study were generated from full-length cDNAs coding for human ENaC subunits cloned in our laboratory (Edelheit et al. 2011). From these clones, we subcloned cDNAs coding for the extracellular domains of α-ENaC (residues 107–561), β-ENaC (residues 72–531) and γ-ENaC (residues 77–541) into pET-46Ek/LIC (Novagen, Madison, WI). The N-termini of the proteins were designed to contain the sequence Met–Ala–6xHis–Val–4xAsp–Lys. The sequences of the clones were verified by sequencing as described (Edelheit et al. 2011).

For expression, pET-46EK/LIC-α-ENaC, pET-46EK/LIC-β-ENaC and pET-46EK/LIC-γ-ENaC were transformed into *E. coli* strain Rosetta2 (DE3) (Novagen, Madison, WI, USA). A 5-ml aliquot of overnight culture of each clone was seeded in 500 ml of LB medium containing 50 μg/ml of ampicillin and grown at 37°C until turbidity reached $A_{600} = 0.7$. For protein induction, isopropylthio-β-galactoside (IPTG) (0.1 mM) was added and incubation continued for 4.5 h at 37°C. The cells were precipitated (3,300×*g*, 20 min) and sonicated in 30 s bursts for a total of 3 min (Vibra cell Sonics, 80% amplitude) in 50 ml of lysis buffer (50 mM Tris–HCl, pH 8.0, 0.1% Triton X-100) containing protease inhibitor cocktail (Roche). The protein pellet obtained after centrifugation (10,000×*g*, 10 min) was resuspended in wash buffer (20 mM Tris–HCl, pH 7.8,

100 mM NaCl, 2 M urea) and precipitated again (10,000×*g*, 10 min). The pellet was re-dissolved in 12 ml of wash buffer containing 8 M of urea at room temperature (RT) and sonicated in 5-s bursts for a total of 30 s (40% amplitude). After centrifugation at 10,000×*g* for 10 min, the supernatant was taken for further analysis. Polyacrylamide gel electrophoresis with sodium dodecyl sulfate (SDS-PAGE) showed a protein of expected size (~50 kDa for α-ENaC) in IPTG-induced cultures but not in uninduced cells.

The major band in the α-ENaC fraction was identified by mass spectrometry as described below. Western blot analysis using a commercially available anti α-ENaC antibody (H-95, Santa Cruz) showed specific reaction with α-ENaC band, but not with *β*- or *γ*-ENaC bands.

Cloning and expression of ENaC subunits in baculovirus Sf9 system

Full-length α-, *β*-, and *γ*-ENaC cDNAs were cloned under the control of polyhedrin promoter in the baculoviral transfer vector, pVL1393, using forward primer 5′-ATCGA CGCGGATCCACCATGGCACATCACCACCACCATC-3′ for α-ENaC, *β*-ENaC and *γ*-ENaC, and reverse primers 5′-GAATCGGCTCTAGAGGTTCAGGGCCCCCCCAGA GG-3′ for α-ENaC, 5′-CACCTAGCTCTAGATTAGATG GCATCACCCTCACTG-3′ for *β*-ENaC and 5′-ACCT AGCTCTAGAGGTTCAGAGCTCATCCAGCATCTG-3′ for *γ*-ENaC. The resulting plasmids were designed to contain N-terminus 6xHis tag.

To produce recombinant baculoviruses (BVs), insect Sf9 cells were cotransfected with baculoviral transfer vectors by mixing 6 µl of Escort transfection reagent (Sigma), 75 µl of culture medium (Expression Systems, USA), 2 µl Flashbac DNA (Oxford Expression Technologies) and 0.5 µg of pVL1393-α-ENaC/pVL1393-*β*-ENaC/pVL1393-*γ*-ENaC. After 15 min of incubation at RT, 610 µl of culture medium was added to each reaction. The reactions were then transferred to a six-well plate containing 1.8×10^6 Sf9 cells per well and incubated for 6 h for BV attachment to the cells. The medium was then aspirated and replaced with fresh 2 ml medium containing penicillin–streptomycin–amphotericin solution (Biological Industries). The viruses were harvested 5 days after infection and kept at 4°C.

BVs were amplified by infecting 12×10^6 Sf9 cells in 12 ml in a 75-ml tissue culture flask and incubated at 27°C for 30 min. The medium was then replaced by 0.5 ml of recombinant BV and 2 ml culture medium and incubated for 1 h. An additional 8 ml culture medium was then added to the flask and incubated for 72 h. The medium was aseptically collected, centrifuged at 500×*g* for 5 min and the supernatant containing recombinant BVs was kept for further amplifications. This amplification procedure was repeated three times, each time using recombinant BV from the previous amplification. Fetal bovine serum was added to the BVs from the final amplification step to a concentration of 2%, filtered through a 0.2-µm filter and divided into 1-ml aliquots for long-term storage at −80°C.

Sf9 insect cells were grown in 40 ml of culture medium in a 250-ml Erlenmeyer flask at a concentration of 2.5×10^6 cells/ml, infected with α-ENaC BV/*β*-ENaC BV/*γ*-ENaC BV and incubated at 27°C for 78 h until they reached a concentration of 10×10^6 cells/ml. At this stage, 70–80% of the cells appeared vital. The cells were harvested by centrifugation at 3,000×*g* for 10 min at 4°C and sonicated in 5-s bursts for a total of 1 min (40% amplitude) in 4 ml of lysis buffer (50 mM Tris–HCl, pH 7.7, 0.1% Triton X-100) containing protease inhibitor cocktail.

In-gel digestion and protein identification by LC–ESI–MS/MS

The protein bands were excised from the polyacrylamide gel stained with Coomassie blue. The protein bands were then reduced, alkylated and digested in gel with bovine trypsin (sequencing grade, Roche Diagnostics, Germany), at a concentration of 12.5 ng/µl in 50 mM of ammonium bicarbonate at 37°C (Shevchenko et al. 1996). The peptide mixtures were extracted with 80% CH_3CN and 1% CF_3COOH, and the organic solvent was evaporated in a vacuum centrifuge. The peptide mixtures were dissolved in 80% formic acid and immediately diluted 1:10 with Milli-Q water prior to the analysis by online reverse-phase nano-liquid chromatography (LC), electro spray ionization (ESI) and tandem mass spectrometric analyses (MS/MS).

Samples were analyzed in LTQ-Orbitrap (Thermo Fisher Scientific, Bremen, Germany) operated in the positive ion mode. Nano-LC–ESI–MS/MS—Peptide mixtures were separated by online reverse-phase nanoscale capillary LC and analyzed by ESI–MS/MS. For the LC–MS/MS, the samples were injected onto an in-house made 15 cm reverse-phase fused-silica capillary column (inner diameter 75 µm, packed with 3-µm ReproSil-Pur C18 A18 media (Dr. Maisch GmbH, Ammerbuch-Entringen, Germany), using an UltiMate 3000 Capillary/Nano-LC System, The LC set-up was connected to the LTQ-Orbitrap mass spectrometer equipped with a nanoelectrospray ion source (Thermo Fisher Scientific, Bremen, Germany). The flow rate through the column was 300 nl/min. An acetonitrile gradient was employed with a mobile phase containing 0.1 and 0.2% formic acid in Milli-Q water in buffers A and B, respectively. The injection volume was 5 µl. The peptides were separated with 50 min gradients from 5 to 65% CH_3CN. The voltage applied to produce an electrospray was 1.3 kV. Helium was introduced as a collision gas at a

pressure of 3 psi. The mass spectrometer was operated in the data-dependent mode. Survey MS scans were acquired in the Orbitrap with the resolution set to a value of 60,000. Up to the seven most intense ions per scan were fragmented and analyzed in the linear trap. For the analysis of tryptic peptides, survey scans were recorded in the FT-mode followed by data-dependent collision-induced dissociation (CID) of the seven most intense ions in the linear ion trap (LTQ). Raw spectra were processed with MASCOT (Matrix Science, London, UK) against an NCBInr database filtered for human sequences. Search parameters included variable modifications of 57.02146 Da (carboxyamidomethylation) on Cys, 15.99491 Da (oxidation) in Met and 0.984016 Da (deamidation) on Asn and Gln. The search parameters were as follows: maximum two missed cleavages, initial precursor ion mass tolerance 10 ppm, fragment ion mass tolerance 0.6 Da. The identities of the peptides were concluded from the detected collision-induced dissociation products by Mascot software and confirmed by manual inspection of the fragmentation series.

Production of antiserum against recombinant α-ENaC

To generate antisera against α-ENaC, a 25-µl aliquot of α-ENaC fraction (150 µg of protein) was emulsified with 0.5 ml of complete Freund's adjuvant and injected at multiple subcutaneous sites to rabbits. Subsequent injections were performed on days 45 and 75 with incomplete Freund's adjuvant. Blood samples were taken 15 days after the second and third injections. Serum was separated from clotted blood cells and stored at −20°C.

Western blot analysis

Tissue samples were frozen and stored at −80°C within 15 min post-operation. Tissues were homogenized (1.5 g tissue/10 ml) in 50 mM Tris, pH 7.4, 1 mM EDTA and protease inhibitor cocktail for 2 min at 4°C and stored at −80°C (Hanukoglu and Hanukoglu 1986). This yielded a homogenate of 20–30 mg protein/ml as determined by Bio-Rad Protein Assay (Bio-Rad) based on the Bradford method using bovine serum albumin (BSA) as standard.

For gel electrophoresis, samples were dissolved in gel sample buffer (0.045 M Tris, pH 6.8, 1% SDS, 10% glycerol, 0.001% Bromophenol Blue and 50 mM dithiothreitol), boiled for 5 min and electrophoresed in 10% polyacrylamide gels. The proteins were transferred to nitrocellulose using a Bio-Rad gel apparatus. The membrane was then incubated in 6.5% non-fat dry milk (Bio-Rad) in phosphate-buffered saline (PBS: 10 mM potassium phosphate, pH 7.4, 150 mM NaCl) at RT for 1 h. Antisera was added at a 1:1,000 dilution and incubated for 1 h. The membrane was then washed four times with PBS + 0.1% Tween-20 (PBST) for 20 min. The membrane was reacted with horseradish peroxidase-conjugated donkey anti-rabbit antibody (Jackson) (1:3,000 dilution) in 5% non-fat dry milk in PBS and then washed four times using PBST for 20 min. The peroxidase-labeled blots were developed using chemiluminescence method with luminol. Nitrocellulose membrane was soaked in 12 ml buffer containing 0.1 M Tris, pH 8.5, 2.5 mM luminol, 400 µm *p*-coumaric acid and 3 µl hydrogen peroxide. After 2 min, the blots were dried on filter paper and visualized by Imagequant las 4,000 mini (General Electric).

Immunohistochemistry and confocal microscopy

Endometrium, ampulla and infundibular regions of the fallopian tube were obtained from patients within 15 min after surgery and immediately fixed in 10% PBS-buffered formalin (Sigma). The endometrial and fallopian tube specimens were from 45 to 66 years old patients who were operated on for benign medical conditions. The bronchial specimens were taken from 82- and 47-year-old males with lung bronchogenic carcinoma. In all cases, the samples were taken from macroscopically preserved areas. The study was approved by the ethics committee at the E. Wolfson Medical Center.

The fixed tissues were incubated for 3 days in 30% sucrose/PBS at 4°C and then stored at −80°C. Frozen tissues were sectioned at −25°C into 15–25 µm-thick sections and kept in PBS containing 0.1% sodium azide at 4°C. The sections were washed with PBS and incubated in PBS containing 2% BSA and 0.1% Triton X-100 at RT for 30 min. The sections were reacted with anti-α-ENaC antiserum (1:100 dilution) and mouse anti-β-tubulin-type IV antibody (1:500 dilution) or monoclonal mouse IgG2A Clone # 24-1 anti-human-CFTR C-terminus antibody (R&D Systems) (1:25 dilution) and incubated overnight at 4°C, and then washed three times with PBS (15 min). Sections were incubated with the secondary antibodies (1:500 dilution), Cy3-conjugated donkey anti-rabbit antibody (Jackson) and DyLight 649-conjugated donkey anti-mouse antibody (Jackson), in PBS with 2% BSA and 0.1% Triton X-100 for 1 h and then washed with PBS for 5 min. To stain the cell nuclei, the sections were also incubated with counterstain 4,6-diamidino-2-phenylindole (DAPI) in PBS for 1 min and then washed twice with PBS. The stained sections were put on slides, dried and mounted with Fluoromount (Sigma).

As a control, sections were incubated as described above but with pre-immune sera instead of the anti-α-ENaC antiserum and without primary anti-β-tubulin-type IV antibody.

Sections were visualized using a Zeiss LSM700 confocal laser scanning microscope with a 63 × 1.4NA Plan-Apochromat or 40 × 1.3NA Plan-Neofluar oil objectives.

The Zeiss LSM 700 was equipped with solid state laser diodes emitting at 405 nm for excitation of DAPI, 555 nm for excitation of Cy3 and DyLight 649 and 633 nm for excitation of DyLight 649 for the ampullary sections that were reacted with anti-ENaC and anti-CFTR antibodies. Stacks consisted of images taken through the z-axis at 0.57-µm step size for the 63× objective and 0.95 µm for the 40× objective using the ZEN 2010 resident acquisition software of the microscope. Pinhole size was adjusted for each channel to the diffraction limit of 1.5 Airy units for the 63× objective and 2.08 Airy units for the 40× objective.

Results and discussion

Novel antibodies specifically identify α-ENaC subunit

In this study to determine the subcellular localization of ENaC, we generated polyclonal antibodies against the extracellular domain of α-ENaC. For this purpose, we isolated α-ENaC fragment expressed in *E. coli* as described under "Methods". The identity of the purified protein as α-ENaC was verified by mass spectrometry. To determine the specificity of the antibodies generated against α-ENaC, we carried out Western blot analysis of human, bovine and mouse tissues known to express α-ENaC (Fig. 1). Total human kidney protein showed one major band with $M_r = 78$ that corresponds to the expected M_r of α-ENaC (75.6). This ENaC subunit undergoes proteolytic processing (Kleyman et al. 2009). The two minor lower bands (M_r 50 and 27) probably represent the processed fragments of α-ENaC. Western blot of total protein from bovine and mouse tissues showed a pattern similar to that observed in human tissues providing further support for the specificity of the antisera (Fig. 1).

The three ENaC subunits are homologous (Saxena et al. 1998). To determine whether antisera cross-react with the other two subunits, we expressed all three proteins separately in Sf9 insect cells in culture. Western blot of total protein isolated from these cells showed no cross-reactivity of the α-ENaC antisera with γ-ENaC. In contrast, β-ENaC showed slight cross-reactivity producing a band with about less than a tenth of the signal intensity observed with α-ENaC (Fig. 1). The identity of the protein recognized by the α-ENaC antisera was further verified by mass-spectral analysis.

ENaC is located on cilia in the fallopian tube

We first examined the expression of ENaC in the female reproductive tract. One of our patients with multi-system PHA due to an Arg508Stop mutation in the α-ENaC gene failed to conceive despite natural and in vitro fertilization attempts for over 4 years. Thus, we hypothesized a connection between the mutation in the α-ENaC gene and infertility.

In the female reproductive system, after ovulation the cumulus–oocyte complex is transferred from the ovary to the funnel-shaped infundibulum end of the oviduct (Fig. 2). Motile cilia in this segment assist in the transfer of the

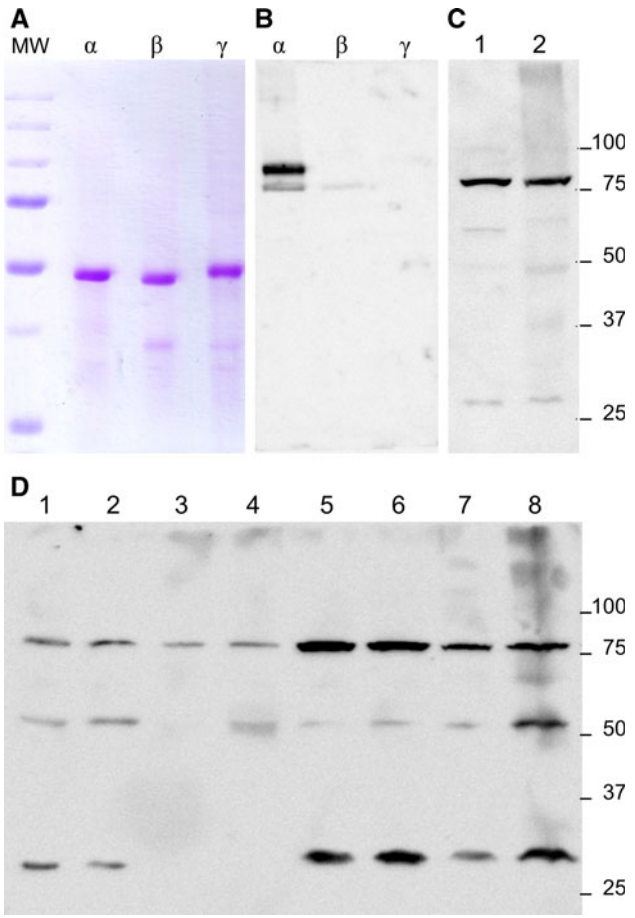

Fig. 1 Purification of extracellular domains (ECD) of ENaC subunits expressed in *E. coli* cells and examination of the specificity of the anti-α-ENaC antibodies by Western blots. **a** Gel electrophoresis of isolated α-, β- and γ-ENaC subunit ECDs expressed in *E. coli* cells (4 µg/lane). **b** Western blots of whole cell lysates of Sf9 cells expressing ENaC subunits (2 µg/lane). *Lane 1* whole α-ENaC + 6x-His (76 kDa) (88 kDa band is probably the glycosylated form of α-ENaC), *lane 2* whole β-ENaC, and *lane 3* whole γ-ENaC. Note that α-ENaC antibody recognizes strongly α-ENaC, and also shows minor cross-reactivity with β-ENaC but not with γ-ENaC. **c** Western blot of total human kidney protein samples (150 µg/lane). The major band at 78 kDa corresponds to the expected size of α-ENaC. Minor lower bands probably represent processed fragments of α-ENaC as previously reported. **d** Western blot of total protein samples (150 µg/lane) from bovine lung (1, 2) and kidney (3, 4), and mouse lung (5, 6) and kidney (7, 8). Three major bands are seen with Mr values of 77–79, 50 and 26–27. The highest band corresponds to the expected Mr of α-ENaC and the lower bands correspond to processed fragments of α-ENaC

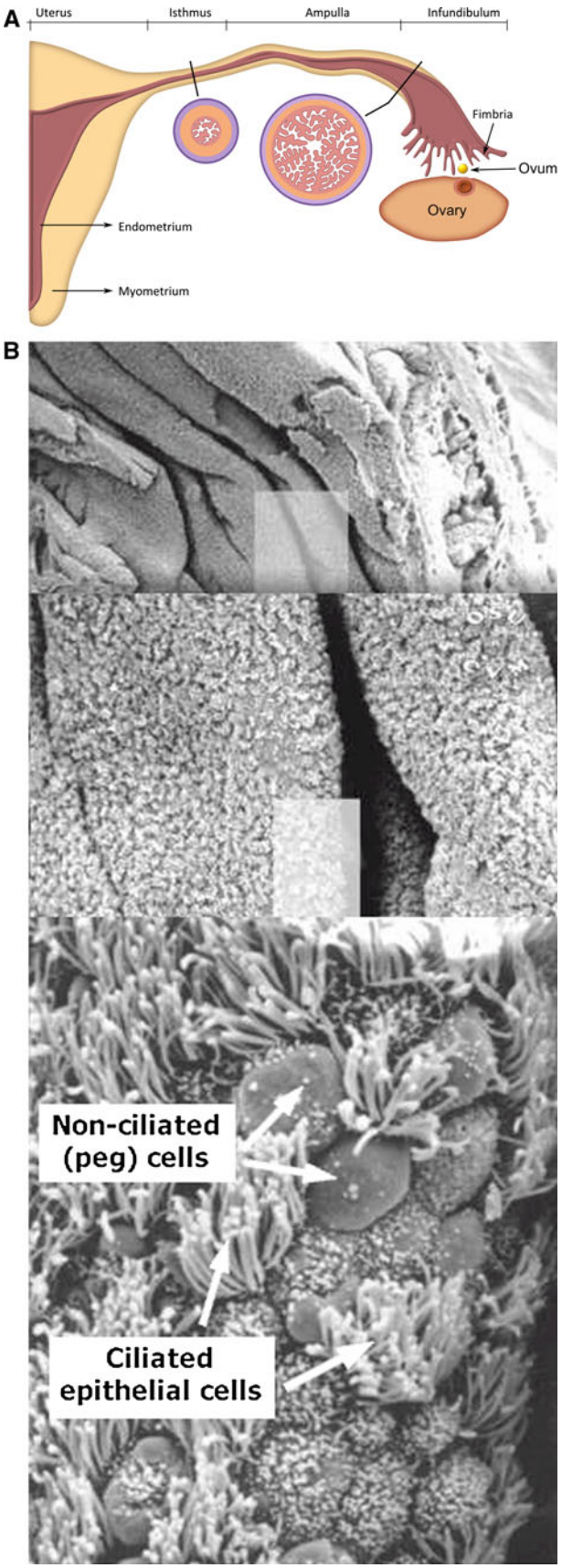

Fig. 2 Schematic view of the human female reproductive tract and ▶ scanning electron micrographs of mouse oviduct. **a** After ovulation, the ovum is transported by fimbriae to the ampulla where fertilization takes place. **b** The epithelia in the ampullary region of mouse oviduct at three levels of magnification. The *light shaded* region is magnified in the lower micrograph (images provided by Dr. Charlotte L. Ownby, Center for Veterinary Health Sciences, Oklahoma State University, Stillwater, Oklahoma, USA)

ovum from the ovary to the middle segment of the oviduct named the ampulla region. Fertilization of the ovum normally occurs in the ampulla, and the fertilized egg is then transported to the uterus for implantation and embryonal development. We examined ENaC expression in three segments of the female reproductive tract: the mucosal layer of the uterus, namely the endometrium, the ampulla of the oviduct and its infundibular end containing fimbriae (Fig. 2).

In this study, we examined the localization of ENaC using anti-α-ENaC antibodies. Previous studies showed that all three subunits were essential for transport and assembly of ENaC on cell surface (Edelheit et al. 2011). Since α-ENaC immunofluorescence on cell surface reflects the presence of a fully assembled heterotrimeric ENaC, here it will be referred to as "ENaC immunofluorescence". In some samples, we also examined immunofluorescence using anti-*β*-ENaC antibodies, which showed results identical to those observed with anti-α-ENaC antibodies (results not shown).

Confocal microscopy of immunofluorescence revealed major transitional changes in the distribution and location of ENaC on epithelia lining the human female reproductive tract. At the fimbrial end of the fallopian tube, ENaC is located on cilia (Fig. 3). Moving from the infundibular segment toward the isthmus, the percentage of multi-ciliated cells gradually decreases (Fig. 4). Finally, at the endometrial end, ENaC is located on the flat apical surfaces of non-ciliated epithelial cells (Fig. 5). As noted below, this distribution of ENaC matches well to serve the physiological functions of the different segments of the reproductive tract.

Three-dimensional (3D) images of fluorescently labeled infundibular epithelia revealed an orderly mosaic of apical surfaces of cells (Fig. 3). To examine the presence of motile cilia, we used cilia-specific anti-*β*-tubulin IV antibodies. In this segment, the majority of the cells express both ENaC (*green*) and *β*-tubulin IV (*red*). In the sample shown here, >95% of the cells were ciliated (Fig. 3). For both ENaC (*green*) and *β*-tubulin IV (*red*), fluorescence was uniformly distributed over the surface of each cell expressing these two proteins. Cell borders on the apical surface were dark, indicating no expression of these proteins at these regions. Consistently, cells that showed no staining for α-ENaC also showed no staining for *β*-tubulin

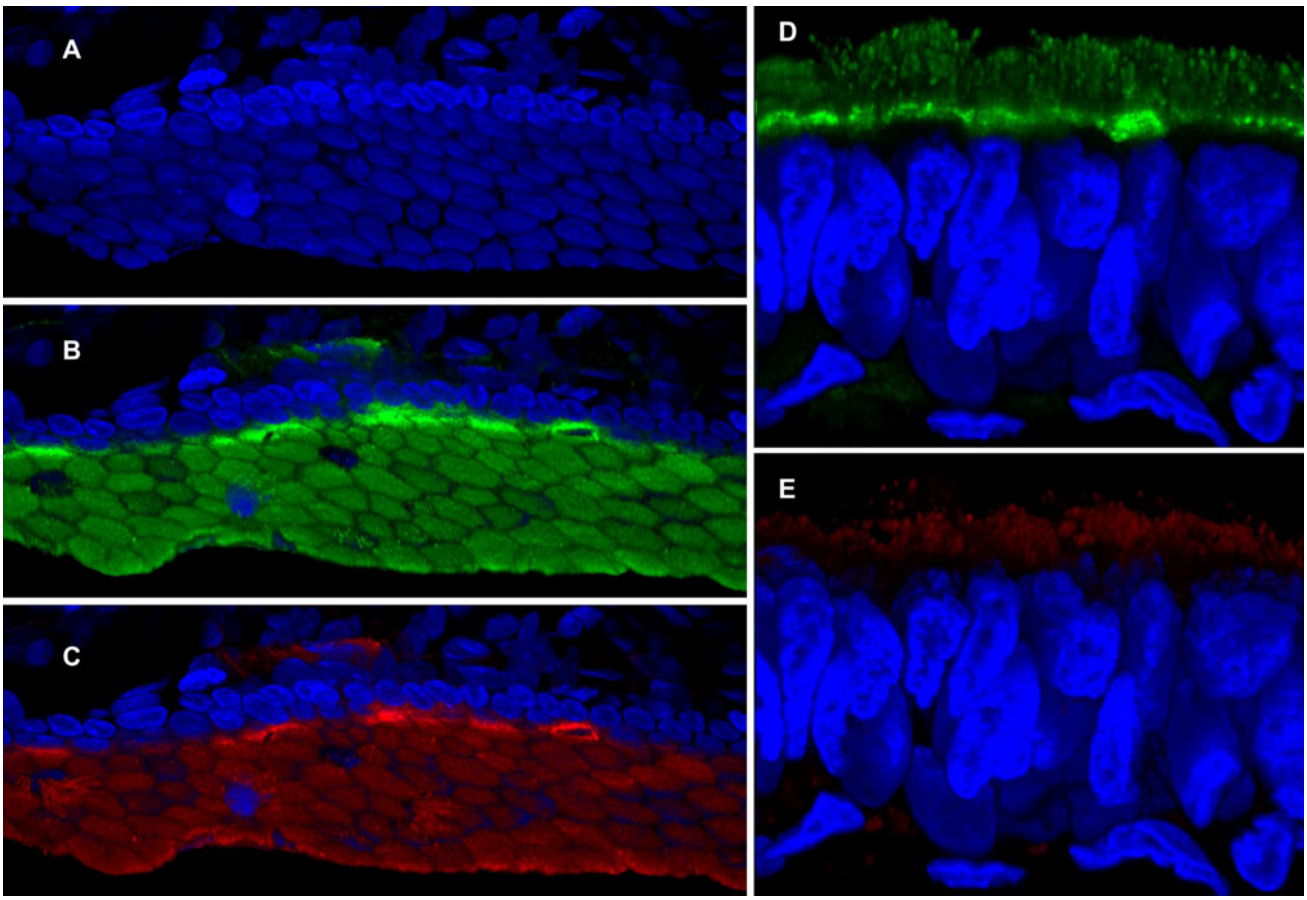

Fig. 3 The wall of epithelia with motile cilia co-expressing α-ENaC and β-tubulin IV in the fimbrial region of the oviduct. **a–c** The section was stained with anti-α-ENaC (*green*), anti-β-tubulin IV antibodies (*red*) and DAPI (*blue*). Note the specificity of expression, the mosaic pattern of apical surface of cells and the tuft-like extensions of cilia on cell surfaces. **d**, **e** Magnified longitudinal section showing motile cilia co-expressing ENaC (*green*) and β-tubulin IV

IV (Fig. 3a, b). At high magnification, the cilia showed strong fluorescence for both α-ENaC and β-tubulin IV. We did not observe any cell with β-tubulin IV that is devoid of α-ENaC.

A previous study reported that in the fimbriae, the percentage of ciliated cells range from 26 to 67% in different subjects with no apparent significant difference between menstrual cycle stages and post-menopausal status (Crow et al. 1994). The reason we observed a higher percentage may be a result of our use of more sensitive method of immunofluorescent display of motile cilia-specific β-tubulin IV, whereas the previous study used light microscopy that might have missed identifying cells with short cilia (Crow et al. 1994).

Immunofluorescence of the ampullary epithelia revealed that ENaC is expressed in large patches of epithelia (Fig. 4). The morphology of ENaC expressing epithelial cells was clearly different from epithelial segments not expressing ENaC. While both ENaC expressing and not expressing segments are simple columnar epithelia type, ENaC expressing segments have more elongated nuclei and thicker epithelial strata (Fig. 4). Ampullary epithelia that expressed ENaC were also observed to show β-tubulin IV-specific immunofluorescence indicating that ENaC expressing cells were ciliated. Yet, even under high magnification, we could not visualize long cilia as seen in the infundibulum (Fig. 3).

In endometrial sections, ENaC immunofluorescence (*green*) was limited to the apical segments of the cells lining the walls of the endometrial glands and the endometrial epithelium (Fig. 5). Three-dimensional imaging of 15–25 μm-thick sections containing three to five layers of cells showed nearly uniform fluorescence on the entire wall of the epithelium, indicating that these epithelial cells uniformly express ENaC (Fig. 5b). The dense, orderly packing of DAPI-stained nuclei reveal that the cells themselves in the epithelial layer are also densely packed. The cells in the connective tissue that have small and widely scattered nuclei show no ENaC expression (Fig. 5b). Under high magnification, epithelial cells show very clearly ENaC expression only on their apical surface (Fig. 5c).

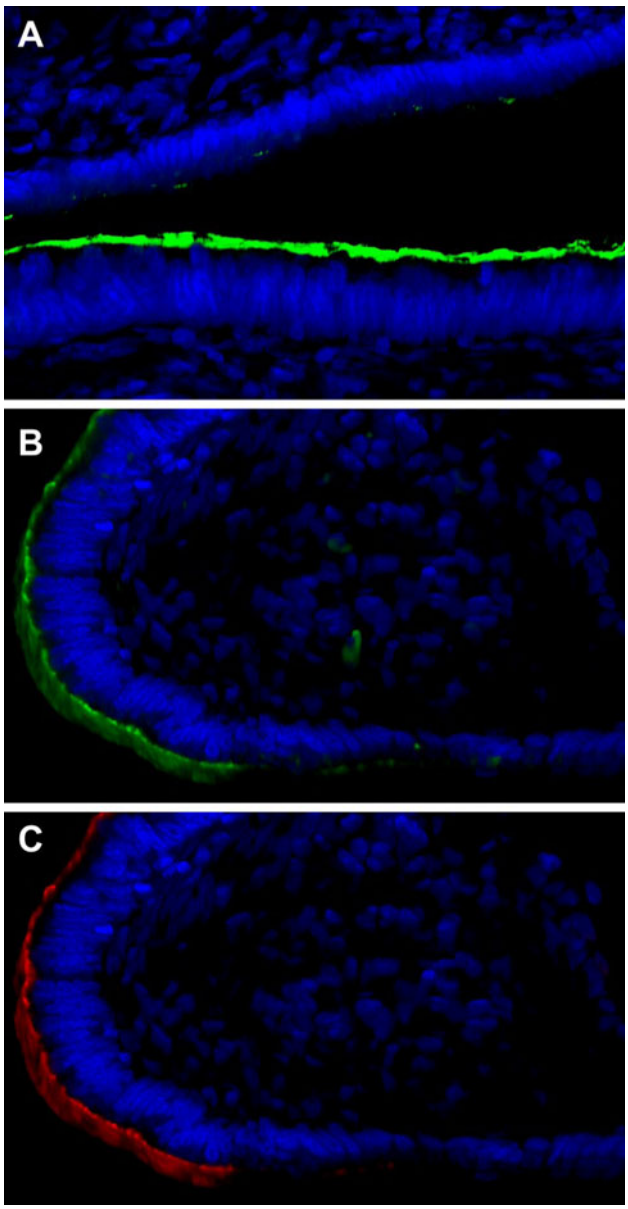

Fig. 4 Distinct epithelia co-expressing α-ENaC and β-tubulin IV in the ampullary region of the oviduct. The sections were stained with anti-α-ENaC and anti-β-tubulin IV antibodies and secondary antibodies labeled with Cy3 (*green*) and DyLight649 (*red*), respectively. The nuclei were stained with DAPI (*blue*). **a** 3D image of a 16 µm-thick section with two neighboring epithelia, the lower one with and the upper one without ENaC expression. **b**, **c** 3D image of a 15 µm-thick section showing co-expression of ENaC (*green*) and β-tubulin IV (*red*). Note that the epithelium co-expressing ENaC and tubulin ends at the same site and the shapes of the epithelial cells to the right of the border are different from those expressing ENaC and tubulin

Overall, endometrial glands showed no fluorescence using cilia-specific anti-β-tubulin IV antibodies. Yet in rare instances in the endometrial sections, we could identify a few multi-ciliated cells stained with this antibody (Fig. 6). Examination of the 3D images of these cases revealed that multi-ciliated cells embedded in the endometrial epithelia have different morphology with rounded and smaller nuclei as opposed to the elongated and larger nuclei of the endometrial gland pseudostratified epithelia (average nucleus size 27.2 and 35.1 µm^2, respectively) (Fig. 6).

Regulation and functions of ENaC in the female reproductive tract

Our results summarized above establish for the first time prominent and uniform distribution of ENaC on cilia in all multi-ciliated cells along the entire female reproductive tract. The function of ENaC, i.e., the transfer of Na^+ from the lumen into the epithelial cell, is the same in all tissues. This action has far reaching consequences as it changes the osmolarity of the extracellular fluid (ECF) and consequently flow of water from the ECF into the cell, and ultimately determines the volume of fluid that bathes the cilia in the lumen. Therefore, ENaC function has to be regulated in a tissue-specific manner consistent with the function of motile cilia.

The female reproductive tract undergoes a series of dynamic changes at each reproductive cycle. At the beginning of the estrous cycle in animals, and the menstrual cycle in females, the ovarian–pituitary–hypothalamic axis hormones stimulate development of ova in the ovary. In parallel, steroid hormones estradiol and progesterone prepare the reproductive tract for the processes of ovum and sperm transport for fertilization, followed by implantation of the embryo in the endometrium. These events are accompanied by major changes in the epithelial lining of the reproductive tract (Crow et al. 1994; Achache and Revel 2006; Jabbour et al. 2006).

After ovulation, the distal fimbrial segment of the fallopian tube sweeps the ovarian surface to move the cumulus–oocyte complex to the fallopian tube (Fig. 2). The rhythmic beating of the cilia is considered to be the major force that transports the cumulus–oocyte complex toward the ampulla (Lyons et al. 2006). Kartagener's syndrome, also known as immotile cilia syndrome, is associated with infertility (Plesec et al. 2008). These cilia could not fulfill their function without periciliary fluid bathing them. ENaC expressed in the fallopian tube must be involved in the regulation of both electrolyte composition and volume of the periciliary fluid. By using RT-PCR, Chan et al. detected ENaC expression in the mouse endometrium but not in the oviduct and concluded that "ENaC does not have a significant role in regulating oviduct fluid homeostasis" (Chan et al. 2002). Our results completely contradict this conclusion. The reason for their results is most likely due to the fact that they examined total tissue RNA, wherein the amount of ENaC expressing cells was below the level of detection. These findings serve as a caveat against the use of total tissue RT-PCR to determine

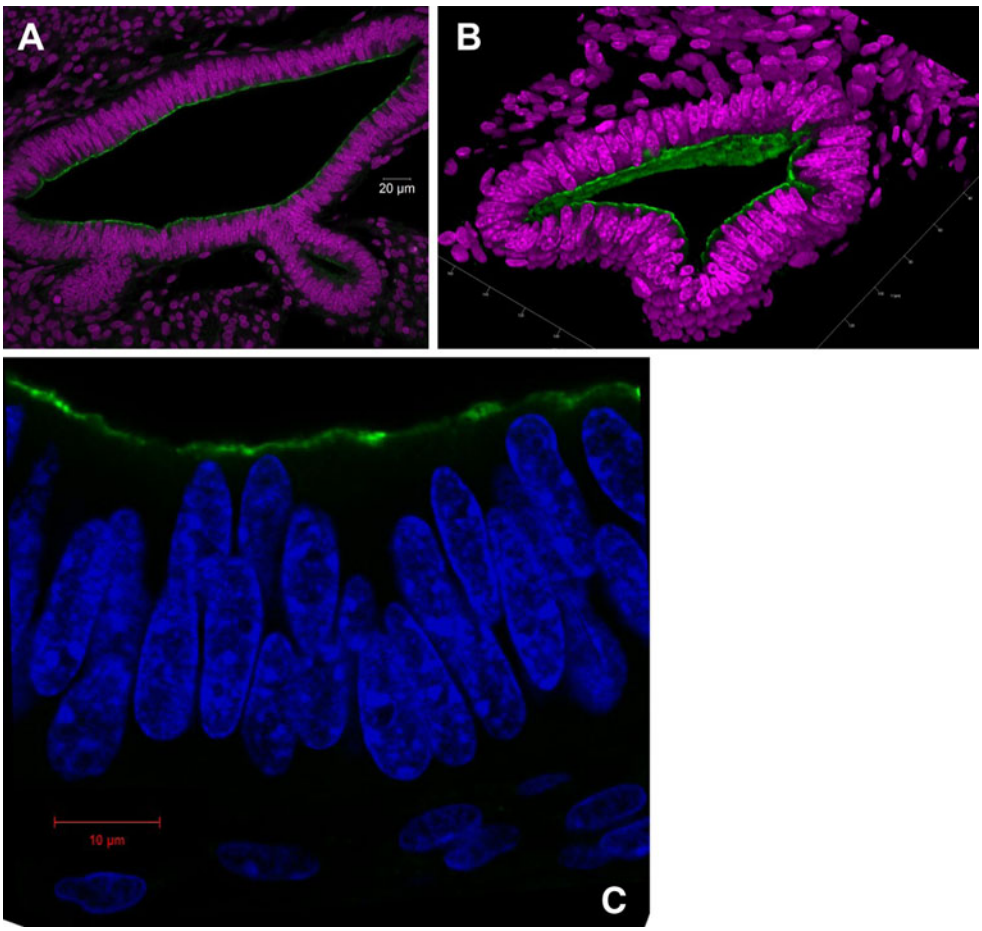

Fig. 5 Apical localization of α-ENaC in human endometrial glands (without motile cilia). Human endometrium sections were stained with anti-α-ENaC antibodies and secondary antibodies labeled with Cy3 (*green*). The nuclei were stained with DAPI. **a** 2D fluorescence micrograph showing uniform distribution of ENaC along the apical border of the epithelium. **b** 3D image showing nearly uniform distribution of ENaC along the apical walls of the gland. **c** Magnified view of the pseudo-stratified epithelium showing strong staining in the apical border

expression in a certain class of epithelial cells that represent a minuscule fraction of tissue sample.

The transport of the cumulus–oocyte complex in the oviduct is critical for the subsequent steps of fertilization and implantation. Prior to ovulation, uterine lumen is fluid filled. This environment is optimal for sperm motility and capacitation. Toward the pre-implantation phase, the uterine luminal fluid is absorbed leading to the closing of the uterus (Salleh et al. 2005). The rapid changes in the luminal fluid levels are probably brought about by changes in the movement of Na^+ ions that tip the balance of osmolarity to affect net movement of fluid across apical membrane. In mouse uterus, α-ENaC and CFTR mRNAs show cyclic changes (Chan et al. 2002). These findings support the hypothesis that up-regulation of ENaC and down-regulation of CFTR are jointly responsible for the re-absorption of uterine fluid in preparation for implantation (Chan et al. 2002; Yang et al. 2004). In the follicular phase of the menstrual cycle, estradiol levels gradually increase. After ovulation, plasma estradiol levels drop and progesterone levels increase. Studies in ovariectomized rats showed that while estradiol stimulated secretion of Na^+, K^+ and water to the uterine lumen, progesterone stimulated the reabsorption of these ions and water (Clemetson et al. 1977). These results further support the hypothesis that the physiological changes are mediated by the action of steroid hormones on ENaC expression.

In conclusion, for the first time we have shown that ENaC is expressed along the entire female oviduct and is localized on cilia in multi-ciliated cells. These results indicate that ENaC plays an important role in the regulation of the ionic composition and volume of periciliary oviductal fluid and support the hypothesis that infertility of PHA patient is a consequence of α-ENaC gene mutation. The average rate of successful implantation after in vitro fertilization (IVF) rate is ∼25% (Achache and Revel 2006). Thus, the present results suggest that more attention should be directed to the examination of fluid and electrolyte homeostasis prior to implantation.

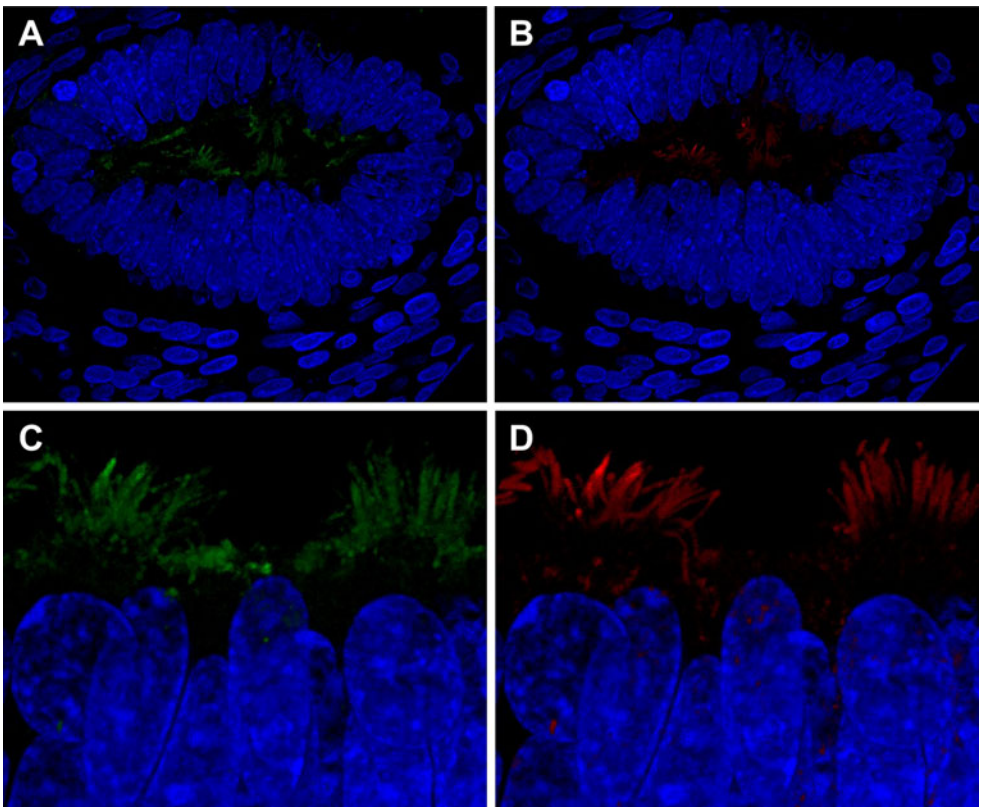

Fig. 6 Rare occurrence of multi-ciliated cells in pseudo-stratified epithelia in human endometrial glands. **a**, **b** 3D image of cross section of a gland stained with anti-α-ENaC (*green*) and anti-*β*-tubulin IV (*red*) antibodies. Note the tufts in the lumen of the gland stained with both antibodies. Paging through the stacks that compose the 3D confocal image, we can clearly identify that the cells that carry the cilia have round nuclei visible in the image. Epithelial cells with the elongated nuclei do not have visible cilia. **c**, **d** Magnified view showing co-expression of ENaC (C) and *β*-tubulin IV (D)

ENaC is located on cilia in the bronchial epithelia

In addition to the female reproductive system, we examined the epithelia of the human bronchus as this is the second major tissue with well-known roles for motile cilia associated with mucous clearance. Immunofluorescence of epithelia from human bronchus revealed a dense image of cilia on the epithelia (Fig. 7). ENaC fluorescence was observed on all cells that expressed cilia-specific *β*-tubulin IV. At high magnification, 3D images revealed round vesicular structures showing both ENaC (*green*) and *β*-tubulin IV fluorescence (Fig. 7c, d). These vesicular structures were seen in the space between the upper border of the nuclei and the apical membrane. We could not visualize similar structures in the lower part of the cells neighboring the basolateral membrane.

Cilia increase cell surface area >70-fold

Using 3D confocal microscopy images, we quantitated some parameters of the epithelial cells with cilia (Table 1). In the fallopian epithelia, we could easily visualize and distinctly localize specific epithelial cell surfaces (Fig. 3). This allowed us to calculate the mean flat surface area of one cell as 14 μm^2. Assuming that the average diameter of the surrounding membrane of a cilium is 260 nm (Williams et al. 2011), the height of the cilium is $\sim$5 μm; and with 250 cilia per cell, the total surface area of cilia in the infundibulum is 964 μm^2 per cell (Table 1). This value is 68-fold higher than the flat surface area of a non-ciliated cell. In other words, cilia increase cell surface area almost 70-fold. The mean length of the cilia in the bronchus was about 50% longer than those in the reproductive tract (7.2 μm vs. $\sim$5.0 μm) (Table 1). Since cilia are 1.4 times longer in the epithelium lining the bronchus, the increase in the cell surface area could be assumed to be even greater there.

Since all the cilia along their entire lengths are furnished with ENaC, assuming the same density of ENaC in ciliated versus non-ciliated cells, the quantity of ENaC on the cell surface should be $\geq$70-fold in ciliated cells.

Another question we examined is the ratio of ENaC located on cilial membrane versus on cell surface patches without cilia. The mean number of cilia per cell is 250. The bases of 250 cilia cover an area of 13.3 μm^2:

$$\text{Area of 250 cilial platforms} = 250 \times 2\pi \times r^2 = 250 \times 3.14 \times 0.13^2 = 13.27\ \mu m^2$$

Since the mean flat surface of a cell is 14.1 μm^2, the remaining area of cell surface that is not covered by cilia is 14.1–13.3 = 0.8 μm^2. Thus, the ratio of cell membrane covering cilia to cell membrane in patches that have no cilia is about 1,200 to 1 (specifically 964/0.8 = 1205). In immunofluorescent staining, we do not see any significant difference in the intensity of fluorescence on cilia versus patches in between cilia. Thus, if ENaC is distributed at

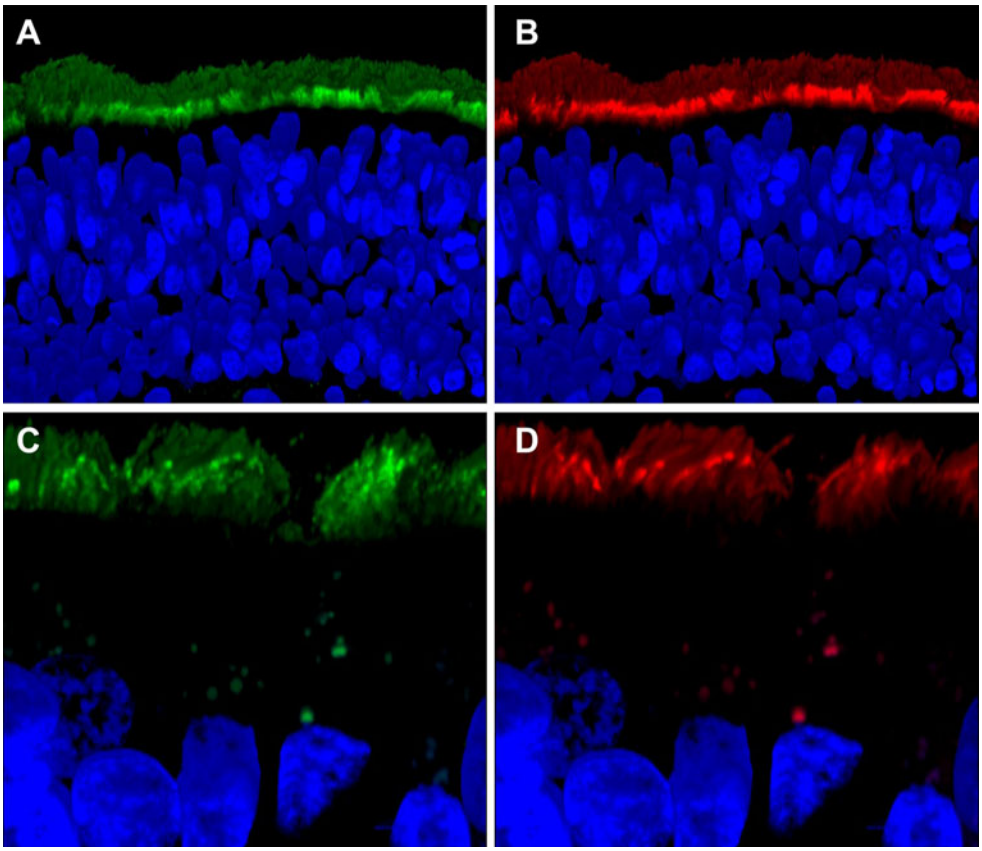

Fig. 7 High expression of ENaC in the densely ciliated epithelia of the human primary bronchus. **a**, **b** 3D image of longitudinal section of the epithelium stained with anti-α-ENaC (*green*) and anti-β-tubulin IV (*red*) antibodies. Note the high density of the cilia relative to (Figs. 5 and 6. **c**, **d** Magnified 3D view showing co-expression of ENaC (*green*) and β-tubulin IV (*red*). Note that in the cytoplasm of the cells, there are vesicular structures that show both ENaC and tubulin staining

Table 1 Characteristics of ENaC expressing epithelial cells with motile cilia

Tissue	Endometrium	Fallopian tube	Bronchus
Epithelium type	Simple columnar, pseudostratified	Simple columnar, pseudostratified	Pseudostratified
Proportion of ciliated cells	Very rare	High	High
ENaC on all cilia	Yes	Yes	Yes
Number of cilia per cell	–	250–300 (Halbert et al. 1997)	200 (Tarran et al. 2006)
Length of cilia (μm)	5.63 ± 0.25	4.72 ± 0.13	7.23 ± 0.36
Flat cell surface area (μm^2)	–	14.1	–
Cilial surface area (μm^2)	–	963.6	–
Distance between membrane and nucleus (μm)	5.45 ± 0.65	4.28 ± 0.45	16.11 ± 0.85
Nucleus area[a] (μm^2)	57.35 ± 1.39	82.28 ± 3.59	39.73 ± 0.77

[a] At the widest diameter of the nucleus

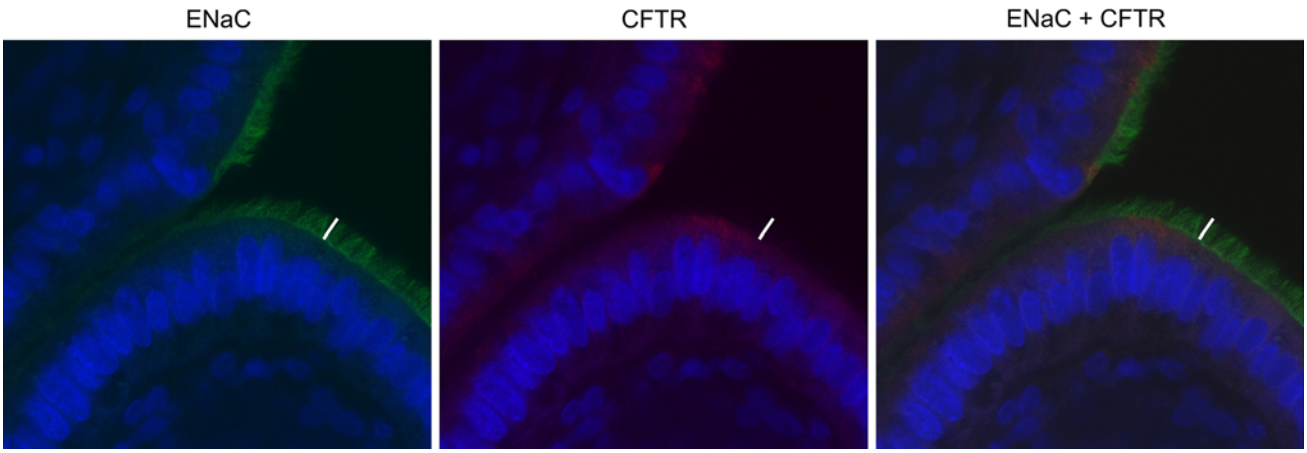

Fig. 8 CFTR is localized on the apical side of epithelial cells, but is not present on cilia in the ampullary region of the oviduct. The sections were stained with anti-α-ENaC (*green*) and anti-CFTR (*red*) antibodies and secondary antibodies labeled with Cy3 (*green*) and DyLight649 (*red*), respectively. The nuclei were stained with DAPI (*blue*). *The short white line* is 7.5-μm long and marks the length of the cilia stained by anti-ENaC. The line is localized at the same position in all images to show that red anti-CFTR staining is not observed in the region of the cilia. In the merged image (ENaC + CFTR), cilia remain *green* colored and show no trace of *yellow-orange* merge color

about equal density over the entire cell membrane surface, for each ENaC on cell surface space in between cilia there should be 1,200 channels on the ciliary membrane surface.

A striking difference was also observed in the distance between the apical membrane and the nucleus between epithelia. In the bronchus epithelia, this distance was nearly three to four times longer than that in cells of the reproductive tract (Table 1).

CFTR is not located on cilia

CFTR functions as a chloride ion channel that funnels Cl^- from the cytoplasm to the epithelial lumen (Riordan 2008). As there are many lines of evidence that CFTR function may influence ENaC activity, we also examined CFTR localization in ciliated epithelia. In the ampullary region of the human oviduct, diffuse but specific immunofluorescence of CFTR was observed on the apical side of the epithelial cells (Fig. 8). However, anti-CFTR dependent staining could not be detected on cilia of the multi-ciliated cells lining the ampulla (Fig. 8). Whereas ENaC immunofluorescence was uniform across cilia, anti-CFTR immunofluorescence showed differential distribution across epithelial cells, some of which had stronger staining close to the apical membrane (Fig. 8). In bronchial epithelia, we could observe strong CFTR immunofluorescence only in scattered cells (Fig. 9). In all cases, CFTR immunofluorescence was limited to the apical membrane and cilia showed no CFTR staining (Fig. 9). A previous study reported CFTR immunoreactivity in the apical membrane of rat oviduct epithelium (Chen et al. 2008). Similarly, in human bronchial epithelial cultures, CFTR immunofluorescence was observed only on the apical cell surface in areas that do not have cilia (Riordan 2008; Kreda and Gentzsch 2011).

ENaC location in cilia requires re-evaluation of the mechanism of action of CFTR and other modulators

Many studies have been directed to examine possible interactions between ENaC subunits and other proteins and enzymes that play regulatory roles within epithelial cells. These studies have been mostly carried in experimental cell systems or heterologous expression systems and have provided evidence that ENaC activity may be affected by direct interaction with other proteins, including: chloride channel CFTR, various kinases that participate in signal transduction pathways, furin-type proteases that may activate ENaC, ubiquitin ligase Nedd4 that leads to proteolysis of ENaC subunits, GTP binding proteins and cytoskeletal proteins that may be involved in the trafficking of ENaC subunits to the cell surface.

In epithelia with motile cilia, the most extensively studied interaction is that between ENaC and CFTR in the respiratory airways. Mutations in CFTR lead to cystic fibrosis (CF) (Riordan 2008). The chronic inflammation observed in this disease is apparently due to enhanced activity of ENaC (in the absence of CFTR) that leads to a reduction in the depth of the periciliary fluid, which is also called airway surface liquid (ASL). The influence of CFTR activity on ENaC function could be a secondary consequence of CFTR channeling of Cl^- ions, or alternatively CFTR could influence ENaC function by directly binding to ENaC. On the basis of studies using fluorescence resonance energy transfer

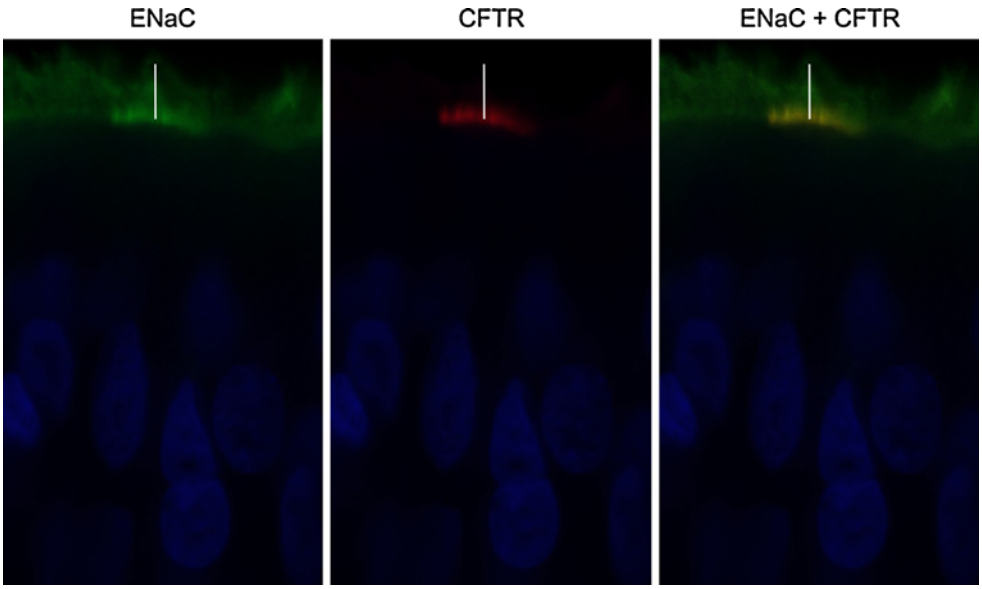

Fig. 9 CFTR is localized on the apical membrane, but is not present on cilia in the human lung bronchus epithelia. The sections were stained with anti-α-ENaC (*green*) and anti-CFTR (*red*) antibodies and secondary antibodies labeled with Cy3 (*green*) and DyLight649 (*red*), respectively. The nuclei were stained with DAPI (*blue*). The *white line* marks the length of the cilia stained by anti-ENaC. The line is localized at the same position in all images. *Red* anti-CFTR staining is not observed in the region of the cilia. In the merged image (ENaC + CFTR), *yellow-orange* merged color appears at the apical membrane level only

(FRET) and co-immunoprecipitation, it has been suggested that CFTR and ENaC interact directly (Berdiev et al. 2009). Our results unequivocally show that the great majority of ENaC is concentrated on cilia in all cells that have motile cilia in both epithelia of the female reproductive tract and respiratory airways (Figs. 4–9), while CFTR is located on apical membrane but not on cilia (Figs. 8–9). Based on these observations, a direct physical interaction between these two complexes would not seem to be a significant event in the respiratory airway epithelia (Fig. 10).

Our measurements and calculations show that only 1 in 1,200 molecules of ENaC is located on the apical cell surface that is devoid of cilia. Thus, there is a chance that 1 in ~1,000 molecules of ENaC could interact directly with CFTR. This possible interaction is probably not sufficient to lead to the full expression of cystic fibrosis symptoms in the absence of CFTR. Yet, our findings do not exclude a direct interaction between CFTR and ENaC in epithelial cells that do not have motile cilia. In cells devoid of motile cilia, as in the endometrium, ENaC is uniformly spread on the apical surface (Fig. 3) and may interact with other apical membrane proteins.

One important class of regulator of ENaC is serine proteases (Kleyman et al. 2009). Membrane-anchored proteases represent a large family of enzymes (Antalis et al. 2010). There is immunohistochemical evidence for the presence of a serine protease in the human airway (Takahashi et al. 2001). There is also evidence that in primary human bronchial epithelial cell cultures, ENaC is activated by proteases (Myerburg et al. 2010). Thus, it is likely that proteases play a role in the regulation of ENaC activity on cilia in vivo.

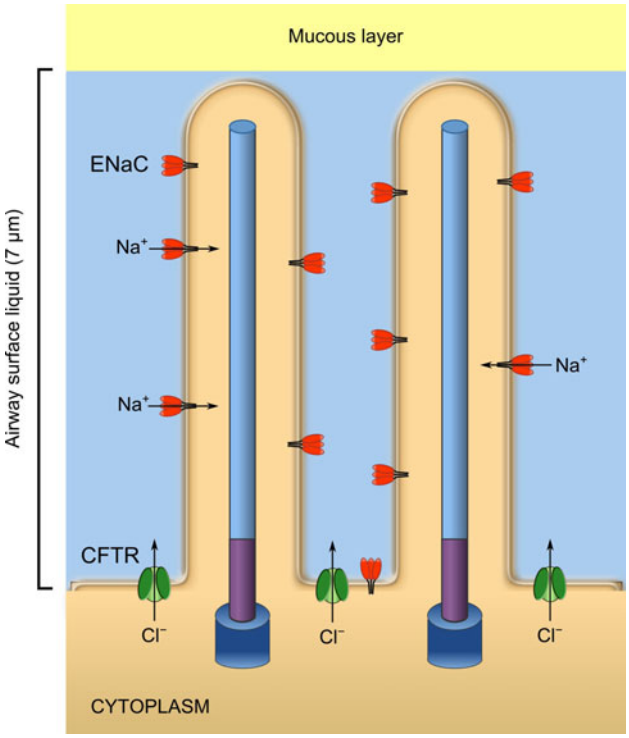

Fig. 10 Graphic model of two motile cilia on human bronchus epithelia showing the locations and functions of ENaC and CFTR on apical cell surface

It should be noted that any mechanism that has been suggested, or will be considered in the future, to explain regulation of ENaC in epithelia with motile cilia should be evaluated taking into consideration that the great majority of ENaC in these cells is located on cilia that constitute a restricted environment.

Physiological reasons for the location of ENaC on cilia

To the best of our knowledge, this is the first study to document abundant and uniform distribution of an ion channel on all motile cilia in different cell types in the two principal tissues, the female reproductive tract and the respiratory airway that have the highest levels of motile cilia. These observations raise some questions: Why is ENaC distribution so widespread and why does ENaC appear over the entire surface of cilia, especially in contrast to CFTR that is another ion channel on the epithelial apical surface?

Although the physiological functions of tissues with motile cilia are vastly different, the motile cilia have the same function and that is muco-ciliary transport. To carry out their function, the cilia need to be in a fluid environment, with a tightly regulated volume and fluid depth. As noted above, prior to implantation, the endometrial lumen is fluid filled, and after ovulation, fluid is reabsorbed "closing" the uterus. The lung malfunction observed in cystic fibrosis is another good example of the need for tight regulation of the fluid where the reduction of the luminal fluid depth by a few micrometers leads to a life-threatening disease.

The volume of fluid in the lumen is regulated by modulation of the osmolar gradient across the cell membrane. Since Na^+ is the major solute in the ECF, enhanced ENaC function decreases osmolarity of the luminal fluid and forces net water flow from the lumen into the epithelial cell. In the opposite direction, the regulating channel is CFTR located on the apical membrane that secretes Cl^- ions from the cytoplasm to the lumen.

We suggest that ENaC-type channels are located over the entire length of cilia for two main reasons: (1) cilial location tremendously increases channel density per cell surface as shown above and (2) cilial location allows channels to serve as sensitive regulators of osmolarity of the periciliary fluid throughout the whole depth of the fluid bathing the cilia. In contrast to ENaC, CFTR does not need to be located on cilia as it secretes Cl^- from the cytoplasm to the lumen.

In conclusion, our results show that in evolution ENaC has been selected as the regulator of fluid volume in all types of mammalian epithelial tissues with motile cilia. Thus, ENaC is involved in all the functions of these epithelia in diverse tissues, including reproductive functions (germ cell transport, fertilization and implantation), clearance of respiratory airways, cell migration and embryonic development.

Acknowledgments This research was funded in part by a grant from the Chief Scientist of the Israel Ministry of Health. The authors thank Mr. Tevie Mehlman (Biological Mass Spectrometry Unit, Weizmann Institute of Science) for assistance with mass spectrometry analysis. This work was carried out in partial fulfillment of the requirements for a Ph.D. degree of Y.E. at the Sackler Faculty of Medicine of Tel Aviv University.

References

Achache H, Revel A (2006) Endometrial receptivity markers, the journey to successful embryo implantation. Hum Reprod Update 12:731–746

Antalis TM, Buzza MS, Hodge KM, Hooper JD, Netzel-Arnett S (2010) The cutting edge: membrane-anchored serine protease activities in the pericellular microenvironment. Biochem J 428:325–346

Berdiev BK, Qadri YJ, Benos DJ (2009) Assessment of the CFTR and ENaC association. Mol Biosyst 5:123–127

Biner HL, Arpin-Bott MP, Loffing J, Wang X, Knepper M, Hebert SC, Kaissling B (2002) Human cortical distal nephron: distribution of electrolyte and water transport pathways. J Am Soc Nephrol 13:836–847

Bourque CW (2008) Central mechanisms of osmosensation and systemic osmoregulation. Nat Rev Neurosci 9:519–531

Boyd C, Naray-Fejes-Toth A (2007) Steroid-mediated regulation of the epithelial sodium channel subunits in mammary epithelial cells. Endocrinology 148:3958–3967

Chan LN, Tsang LL, Rowlands DK, Rochelle LG, Boucher RC, Liu CQ, Chan HC (2002) Distribution and regulation of ENaC subunit and CFTR mRNA expression in murine female reproductive tract. J Membr Biol 185:165–176

Chang SS, Grunder S, Hanukoglu A, Rosler A, Mathew PM, Hanukoglu I, Schild L, Lu Y, Shimkets RA, Nelson-Williams C, Rossier BC, Lifton RP (1996) Mutations in subunits of the epithelial sodium channel cause salt wasting with hyperkalaemic acidosis, pseudohypoaldosteronism type 1. Nat Genet 12:248–253

Chen M, Du J, Jiang W, Zuo W, Wang F, Li M, Chan H, Zhou W (2008) Functional expression of cystic fibrosis transmembrane conductance regulator in rat oviduct epithelium. Acta Biochim Biophys Sin 40:864–872

Clemetson CA, Verma UL, De Carlo SJ (1977) Secretion and reabsorption of uterine luminal fluid in rats. J Reprod Fertil 49:183–187

Crow J, Amso NN, Lewin J, Shaw RW (1994) Morphology and ultrastructure of fallopian tube epithelium at different stages of the menstrual cycle and menopause. Hum Reprod 9:2224–2233

Duc C, Farman N, Canessa CM, Bonvalet JP, Rossier BC (1994) Cell-specific expression of epithelial sodium channel alpha, beta, and gamma subunits in aldosterone-responsive epithelia from the rat: localization by in situ hybridization and immunocytochemistry. J Cell Biol 127:1907–1921

Edelheit O, Hanukoglu I, Gizewska M, Kandemir N, Tenenbaum-Rakover Y, Yurdakok M, Zajaczek S, Hanukoglu A (2005) Novel mutations in epithelial sodium channel (ENaC) subunit genes and phenotypic expression of multisystem pseudohypoaldosteronism. Clin Endocrinol (Oxf) 62:547–553

Edelheit O, Hanukoglu I, Shriki Y, Tfilin M, Dascal N, Gillis D, Hanukoglu A (2010) Truncated beta epithelial sodium channel

(ENaC) subunits responsible for multi-system pseudohypoaldosteronism support partial activity of ENaC. J Steroid Biochem Mol Biol 119:84–88

Edelheit O, Hanukoglu I, Dascal N, Hanukoglu A (2011) Identification of the roles of conserved charged residues in the extracellular domain of an epithelial sodium channel (ENaC) subunit by alanine mutagenesis. Am J Physiol Renal Physiol 300:F887–F897

Gaillard D, Hinnrasky J, Coscoy S, Hofman P, Matthay MA, Puchelle E, Barbry P (2000) Early expression of beta- and gamma-subunits of epithelial sodium channel during human airway development. Am J Physiol Lung Cell Mol Physiol 278:L177–L184

Halbert SA, Patton DL, Zarutskie PW, Soules MR (1997) Function and structure of cilia in the fallopian tube of an infertile woman with Kartagener's syndrome. Hum Reprod 12:55–58

Hanukoglu I, Hanukoglu Z (1986) Stoichiometry of mitochondrial cytochromes P-450, adrenodoxin and adrenodoxin reductase in adrenal cortex and corpus luteum. Implications for membrane organization and gene regulation. Eur J Biochem 157:27–31

Hanukoglu A, Bistritzer T, Rakover Y, Mandelberg A (1994) Pseudohypoaldosteronism with increased sweat and saliva electrolyte values and frequent lower respiratory tract infections mimicking cystic fibrosis. J Pediatr 125:752–755

Helve O, Janer C, Pitkanen O, Andersson S (2007) Expression of the epithelial sodium channel in airway epithelium of newborn infants depends on gestational age. Pediatrics 120:1311–1316

Hildebrandt F, Benzing T, Katsanis N (2011) Ciliopathies. N Engl J Med 364:1533–1543

Hu JC, Bengrine A, Lis A, Awayda MS (2009) Alternative mechanism of activation of the epithelial Na+ channel by cleavage. J Biol Chem 284:36334–36345

Hummler E, Barker P, Gatzy J, Beermann F, Verdumo C, Schmidt A, Boucher R, Rossier BC (1996) Early death due to defective neonatal lung liquid clearance in alpha-ENaC-deficient mice. Nat Genet 12:325–328

Ishikawa H, Marshall WF (2011) Ciliogenesis: building the cell's antenna. Nat Rev Mol Cell Biol 12:222–234

Jabbour HN, Kelly RW, Fraser HM, Critchley HO (2006) Endocrine regulation of menstruation. Endocr Rev 27:17–46

Kashlan OB, Kleyman TR (2011) ENaC structure and function in the wake of a resolved structure of a family member. Am J Physiol Renal Physiol 301:F684–F696

Kerem E, Bistritzer T, Hanukoglu A, Hofmann T, Zhou Z, Bennett W, MacLaughlin E, Barker P, Nash M, Quittell L, Boucher R, Knowles MR (1999) Pulmonary epithelial sodium-channel dysfunction and excess airway liquid in pseudohypoaldosteronism. N Engl J Med 341:156–162

Kleyman TR, Carattino MD, Hughey RP (2009) ENaC at the cutting edge: regulation of epithelial sodium channels by proteases. J Biol Chem 284:20447–20451

Kreda SM, Gentzsch M (2011) Imaging CFTR protein localization in cultured cells and tissues. Methods Mol Biol 742:15–33

Lange K (2011) Fundamental role of microvilli in the main functions of differentiated cells: outline of an universal regulating and signaling system at the cell periphery. J Cell Physiol 226: 896–927

Li C, Naren AP (2010) CFTR chloride channel in the apical compartments: spatiotemporal coupling to its interacting partners. Integr Biol (Camb) 2:161–177

Lyons RA, Saridogan E, Djahanbakhch O (2006) The reproductive significance of human fallopian tube cilia. Hum Reprod Update 12:363–372

Marshall WF, Kintner C (2008) Cilia orientation and the fluid mechanics of development. Curr Opin Cell Biol 20:48–52

Masilamani S, Kim GH, Mitchell C, Wade JB, Knepper MA (1999) Aldosterone-mediated regulation of ENaC alpha, beta, and gamma subunit proteins in rat kidney. J Clin Invest 104:R19–R23

Myerburg MM, Harvey PR, Heidrich EM, Pilewski JM, Butterworth MB (2010) Acute regulation of the epithelial sodium channel in airway epithelia by proteases and trafficking. Am J Respir Cell Mol Biol 43:712–719

Plesec TP, Ruiz A, McMahon JT, Prayson RA (2008) Ultrastructural abnormalities of respiratory cilia: a 25-year experience. Arch Pathol Lab Med 132:1786–1791

Riordan JR (2008) CFTR function and prospects for therapy. Annu Rev Biochem 77:701–726

Rohatgi R, Snell WJ (2010) The ciliary membrane. Curr Opin Cell Biol 22:541–546

Rossier BC, Stutts MJ (2009) Activation of the epithelial sodium channel (ENaC) by serine proteases. Annu Rev Physiol 71:361–379

Salleh N, Baines DL, Naftalin RJ, Milligan SR (2005) The hormonal control of uterine luminal fluid secretion and absorption. J Membr Biol 206:17–28

Satir P, Christensen ST (2007) Overview of structure and function of mammalian cilia. Annu Rev Physiol 69:377–400

Saxena A, Hanukoglu I, Strautnieks SS, Thompson RJ, Gardiner RM, Hanukoglu A (1998) Gene structure of the human amiloride-sensitive epithelial sodium channel beta subunit. Biochem Biophys Res Commun 252:208–213

Shah AS, Ben-Shahar Y, Moninger TO, Kline JN, Welsh MJ (2009) Motile cilia of human airway epithelia are chemosensory. Science 325:1131–1134

Shevchenko A, Wilm M, Vorm O, Mann M (1996) Mass spectrometric sequencing of proteins silver-stained polyacrylamide gels. Anal Chem 68:850–858

Song Y, Namkung W, Nielson DW, Lee JW, Finkbeiner WE, Verkman AS (2009) Airway surface liquid depth measured in ex vivo fragments of pig and human trachea: dependence on Na+ and Cl− channel function. Am J Physiol Lung Cell Mol Physiol 297:L1131–L1140

Strautnieks SS, Thompson RJ, Hanukoglu A, Dillon MJ, Hanukoglu I, Kuhnle U, Seckl J, Gardiner RM, Chung E (1996) Localisation of pseudohypoaldosteronism genes to chromosome 16p12.2-13.11 and 12p13.1-pter by homozygosity mapping. Hum Mol Genet 5:293–299

Takahashi M, Sano T, Yamaoka K, Kamimura T, Umemoto N, Nishitani H, Yasuoka S (2001) Localization of human airway trypsin-like protease in the airway: an immunohistochemical study. Histochem Cell Biol 115:181–187

Takei Y (2000) Comparative physiology of body fluid regulation in vertebrates with special reference to thirst regulation. Jpn J Physiol 50:171–186

Tarran R, Trout L, Donaldson SH, Boucher RC (2006) Soluble mediators, not cilia, determine airway surface liquid volume in normal and cystic fibrosis superficial airway epithelia. J Gen Physiol 127:591–604

Widdicombe JH (2002) Regulation of the depth and composition of airway surface liquid. J Anat 201:313–318

Williams CL, Li C, Kida K, Inglis PN, Mohan S, Semenec L, Bialas NJ, Stupay RM, Chen N, Blacque OE, Yoder BK, Leroux MR (2011) MKS and NPHP modules cooperate to establish basal body/transition zone membrane associations and ciliary gate function during ciliogenesis. J Cell Biol 192:1023–1041

Yang JZ, Ajonuma LC, Tsang LL, Lam SY, Rowlands DK, Ho LS, Zhou CX, Chung YW, Chan HC (2004) Differential expression and localization of CFTR and ENaC in mouse endometrium during pre-implantation. Cell Biol Int 28:433–439

Zhou Z, Duerr J, Johannesson B, Schubert SC, Treis D, Harm M, Graeber SY, Dalpke A, Schultz C, Mall MA (2011) The ENaC-overexpressing mouse as a model of cystic fibrosis lung disease. J Cyst Fibros 10(Suppl 2):S172–S182